J. Min. Metall. Sect. B-Metall. 54 (1) B (2018) 111 - 118

Journal of Mining and Metallurgy, Section B: Metallurgy

THERMODYNAMIC MODELING OF THE Hf-N SYSTEM

M. Pang [a], Y. Peng [b,*], P. Zhou [c], Y. Du [a]

[a] Central South University, State Key Lab of Powder Metallurgy, Changsha, China
[b] Hunan University of Technology, College of Metallurgy and Material Engineering, Zhuzhou, China
[c] Hunan University of Science and Technology, School of Mechanical and Electrical Engineering, Xiangtan, China

(Received 20 May 2017; accepted 21 December 2017)

Abstract

Hf-N based alloys have been widely used and studied in the fields of electronic devices and cutting tools industry. A thermodynamic description of this system is essential for further materials development. By means of CALPHAD method, a thermodynamic modeling of the Hf-N system was carried out based on the available phase diagram data as well as thermodynamic property data. The Fcc phase is modeled as $(Hf, Va)_1(N, Va)_1$ to cover the composition range since the solubility of nitrogen in Fcc phase is reported up to about 52 at.%. A set of self-consistent thermodynamic parameters for the Hf-N system has been obtained. The computed phase diagrams and thermodynamic quantities using the present parameters agree well with the experimental data.

Keywords: *CALPHAD; Hf-N; Phase diagram; Hafnium nitrides.*

1. Introduction

Transition metal nitrides are widely used in the fields of electronic devices and cutting tools industry due to their excellent properties [1-3]. The close-packed NaCl structure of transition metal nitrides hampers the migration of species and gives rise to excellent thermal stability against oxidation or self-diffusion [4, 5]. Among them, hafnium mono-nitride (HfN_x) has the highest melting point and thus becomes a potential material to be used in harsh environments [6]. Also, HfN_x possesses high electrical conductivity, large "phononic band gap", small real permittivity and high hardness [7-10]. These properties make HfN_x a very promising candidate as counter electrode in dye sensitized solar cells [11], diffusion barrier in electronic devices [12], and protective coating to prevent abrasion and corrosion [13, 14]. HfN is inherent super-conductor with relatively high Tc 8.8 K [8].

For the above reasons, the Hf-N system has been the focus of many theoretical and experimental studies [5, 7, 9, 13, 15-17]. These studies mainly investigated the thermal, mechanical, electronic and optical properties and microstructures of the HfN_x films or Hf-N alloys. It is well known that a phase diagram can provide efficient guides on materials researches. Although the phase equilibria and thermodynamic properties have been investigated by several studies, there is no thermodynamic description of the Hf-N system so far. Thus, this work aims to critically review the experimental data and obtain a set of thermodynamic parameters to describe the Hf-N system via the CALPHAD method. The present work is also a continuing effort of our previous attempts [18] to establish a thermodynamic database for cemented carbides.

2. Evaluation of experimental data

The previous experimental phase diagrams and thermodynamic data of the Hf-N system have been reviewed by Okamoto [19]. However, a few years latter, Lengauer et al. [20] proposed a different phase diagram based on their new experimental data obtained from diffusion couples. All the experimental data as well as first-principles calculated results discussed below are listed with quoted modes in Table 2.

2.1 Phase diagram data

According to Krikorian and Wallace [21], the addition of N stabilizes the Hcp phase. This is confirmed by the results reported by Booker and Brukl [22]. The Hcp solid solution with about 28 at. % N peritectically melts to form liquid plus Fcc phases at 2911 °C [22]. The solubility of nitrogen in hafnium at 2100 °C is about 25.5 at. % N according to the lattice parameter variations of the hexagonal hafnium

*Corresponding author: pengyingbiao1987@163.com

DOI:10.2298/JMMB170520055P

solid solution [22]. The solubility of N in Hcp phase at 1700 °C is about 29 at. % N measured by the same method [23]. Lengauer et al. [20] determined the solubility of N in Hcp phase to be 29.7 at. % N from 1300 to 1800 °C by using diffusion couples and electron probe microanalysis (EPMA) techniques. The transformation between Hcp and Bcc phases exists within the composition range of 1-3 at. % N shown by the DTA measurements [22]. The temperature of the eutectic reaction among liquid, Hcp and Bcc phases is 2190 °C [22]. However, there is no experimental data on the solubility of nitrogen in Bcc phase and thus neglected in the present modeling.

The melting point of Fcc phase is 3000 °C according to Nowotny et al. [24]. However, Booker and Brukl [22] reported that the congruent melting point of Fcc phase is 3387 °C at 49 at. % N under 2 bar pressure of Ar. The pressure dependence of the melting point of the Fcc phase with the composition of $HfN_{0.99}$ under the N_2 pressure range from 0.01 to 80 bar was measured by Eron'yan et al. [25], who observed a linear relationship between $lgP(N_2)$ and $1/T_m$. Ettmayer et al. [26] also measured the melting point of Fcc phase along with various compositions under N_2 pressures from 1 to 15 bar. Comparing with the results of Eron'yan et al. [25], their values of the melting points are doubtful because they are too low which is also found and reported in the assessments of Ti-N [27] and V-N [28] systems. Rudy and Benesovsky [23] concluded that the homogeneity range of Fcc phase is 42.6-52.5 at. % N by measuring the lattice parameter variations. Booker and Brukl [22] proposed that the Hf-rich side of the Fcc phase extends to 43, 40 and 34 at. % N at 1500, 2100 and 2911 °C, respectively. The diffusion couples and EPMA results of Lengauer et al. [20] showed that the homogeneity range of Fcc phase is 41.5-52.0 at. % N from 1300 to 1800 °C. Storms [29] suggested that the Fcc phase is stable at least to 53 at. % N.

There is a compound Hf_2N in equilibrium with Fcc phase according to Rudy and Benesovsky [23]. However, Rudy's subsequent investigation [30] on 33-47 at. % N alloys revealed that there are two closely related compounds in this composition range, Hf_3N_2 and Hf_4N_3, instead of Hf_2N. They pointed out that Hf_3N_2 and Hf_4N_3 are unstable above 2000 and 2300 °C, respectively [30]. Booker and Brukl [22] observed a reaction among Hcp, Fcc and Hf_2N at 1970 °C, which is identified as Hcp + Fcc = Hf_3N_2 considering the results reported by Rudy [30]. Both Hf_3N_2 and Hf_4N_3 are substantially deficient in nitrogen and the compositions should be $Hf_3N_{1.69}$ and $Hf_4N_{2.56}$, respectively [30]. The X-ray investigations from Billy and Teyssedre [31] showed that Hf_3N_2 is in equilibrium with Fcc phase from 800 to 1200 °C, indicating that Hf_4N_3 may be unstable at low temperatures. However, Lengauer et al. [20] argued that Hf_4N_3 is stable at low temperatures, because the wedge-type Hf sample which was reacted in N_2 at 1160 °C for about 500 h, cooled to room temperature and re-heated again to 1160 °C for about 500 h, did form Hf_4N_3. Furthermore, they pointed out that the heat treatment time of 100 h for Hf/HfN mixtures at 1200 °C is not enough to reach equilibrium, and this is the reason why Billy and Teyssedre [31] did not detect Hf_4N_3 with XRD. The composition ranges of Hf_3N_2 and Hf_4N_3 are 34.9-37.2 at. % N and 38.9-39.6 at. % N, respectively [20], which are narrow and are ignored in the present modeling.

Table 1. *Summary of the phase diagram and thermodynamic data of the Hf-N system.*

Type of data	Method[a]	Quoted mode[b]	Ref.
Phase diagram data	OM, XRD, DTA, CA, IM	■	[22]
	DC, EPMA	⊗	[20]
Heat capacity	DSC	■	[33]
	FP	□	[9, 15, 34]
Enthalpy of formation	CM	■	[38]
	FP	□	[10, 39]
P_{N2} over fcc phase	KE, CA	■	[36, 37]
H_T-H_{298}	HTC	■	[35]
Phase stability	IM	■	[25]
	IM	⊗	[26]

[a] For the experimental techniques: OM = Optical metallography; XRD = X-ray diffraction; CA = Chemical analysis; DTA = Differential thermal analysis; IM = Incipient melting; DC = Diffusion couple; FP = First-principles calculation; CM = Combustion measurement; KE = Knudsen effusion; HTC = High-temperature calorimetry; [b] Indicates whether the data were used or not in the optimization process: ■ used; □ compared with; ⊗ not used.

2.2 Thermodynamic data

The heat capacity of Fcc phase at the composition of $HfN_{1.0}$ has been reported by Schick [32]. Lengauer et al. [33] measured the heat capacity of Fcc phase at $HfN_{1.0}$ by using differential scanning calorimeter (DSC) and compared their results with the data reported by Schick [32]. The two sets of heat capacity were very close to each other. Lu et al. [9], Wang et al. [34] and Saha et al. [15] calculated the heat capacity of Fcc phase using first-principles method. The relative enthalpies (H_T-H_{298}) of $HfN_{0.95}$ and $HfN_{1.09}$ in the temperature range between 1200 and 2250 K were reported by Litvinenko et al. [35]. Kibler et al. [36, 37] measured the partial equilibrium nitrogen pressures (P_{N2}) over the Fcc phase at various

temperatures and compositions. They conducted five sets of experiments to determine the P_{N2} over the Fcc phase. However, as they analyzed in the reports, only two sets of results are reliable. Humphrey [38] determined the heat of formation for hafnium mono-nitride at 298 K to be 184.6±0.7 kJ/mol-atoms by combustion calorimetry. The enthalpy of formation for $HfN_{1.0}$ at 298 K calculated by Mulokozi [39] was -187.23 kJ/mol-atoms. By means of first-principles method, Gu et al. [10] calculated the enthalpy of formation for Fcc phase at the composition of $HfN_{1.0}$ to be -1.842 eV (-177.7 kJ/mol-atoms).

3. Thermodynamic models

The Hf-N system contains 7 phases: Hcp, Bcc, Hf_3N_2, Hf_4N_3, Fcc, liquid and gas. The crystal structures of the solid phases are listed in Table 2.

Table 2. *Crystal structures of the solid phases in the Hf-N system.*

Phase	Pearson Symbol Space Group Prototype	Lattice Parameters / pm	References
Hcp (αHf)	hP2 $P6_3/mmc$ Mg	a = 319.46 c = 505.11	[45]
Bcc (βHf)	cI2 Im-3m W	a = 362.5	[46]
Fcc (HfN)	cF8 Fm-3m NaCl	a =452.5	[47]
Hf_3N_2	hR6 R-3m -	a=320.6 c=2326	[30]
Hf_4N_3	hR8 R-3m C_3V_4	a=321.4 c=3112	[30]

3.1 Unary phases

The Gibbs energies of pure elements Hf and N are taken from the SGTE-compilation by Dinsdale [40] and described by an equation of the form:

$$G_i(T) - H_i^{SER} = A + B\cdot T + C\cdot T\cdot \ln T + D\cdot T^2 + E\cdot T^{-1} + F\cdot T^3 + I\cdot T^7 + J\cdot T^{-9} \quad (1)$$

in which H_i^{SER} is the molar enthalpy of the element *i* at 298.15 K and 1 bar in its standard element reference (SER) state, and *T* is the absolute temperature. The last two terms in Eq. (1) are used only outside the ranges of the melting point, i.e., $I\cdot T^7$ is for liquid phase below the melting point, while $J\cdot T^{-9}$ for the solid phases above the melting point.

3.2 Solution phase

The liquid phase is modeled as a completely disordered solution. The Gibbs energy is described by the Redlich-Kister (R-K) polynomial [41]:

$$G_m^{\phi} - H^{SER} = x_N\cdot {}^0G_N^{\phi} + x_{Hf}\cdot {}^0G_{Hf}^{\phi} + R\cdot T\cdot [x_N\cdot \ln x_N + x_{Hf}\cdot \ln x_{Hf}] + x_N\cdot x_{Hf}\cdot \sum_{j=0}^{n} L_{N,Hf}^{j,\phi}(x_N - x_{Hf})^j \quad (2)$$

where $x_N\cdot {}^0G_N^{\phi} + x_{Hf}\cdot {}^0G_{Hf}^{\phi}$ denotes the mechanical mixing of the pure elements N and Hf. $R\cdot T\cdot [x_N\cdot \ln x_N + x_{Hf}\cdot \ln x_{Hf}]$ stands for the contribution of the ideal entropy of mixing to the Gibbs energy. $x_N\cdot x_{Hf}\cdot \sum_{j=0}^{n} L_{N,Hf}^{j,\phi}(x_N - x_{Hf})^j$ represents the excess Gibbs energy. $L_{N,Hf}^{j,\phi}$ is the *j*th R-K parameter of solution phase ϕ, which is expressed as:

$$L_{N,Hf}^{j,\phi} = a_j + b_j\cdot T \quad (3)$$

in which the interaction parameters a_j and b_j are to be optimized based on the experimental phase diagram data and (or) thermodynamic data. H^{SER} is the abbreviation of $x_N H_N^{SER} + x_{Hf} H_{Hf}^{SER}$.

For the terminal solid solution phases Hcp (αHf) and Bcc (βHf), N atoms occupy the interstitial sublattice. Thus, Hcp and Bcc phases are modeled as $(Hf)_1(N,Va)_m$, where m equals to 0.5 for Hcp phase and 3 for Bcc phase. According to the formula for the sublattice model, the Gibbs energy of phase ϕ (ϕ = Hcp or Bcc) can be expressed as:

$$G_m^{\varphi} - H^{SER} = y'_{Hf}\cdot y''_{Va}\,{}^0G_{Hf:Va}^{\varphi} + y'_{Hf}\cdot y''_N\,{}^0G_{Hf:N}^{\varphi} + m\cdot R\cdot T\cdot [y''_{Va}\cdot \ln y''_{Va} + y''_N\cdot \ln y''_N] + y''_{Va}\cdot y''_N\cdot \sum_{j=0}^{n} L_{Hf:N,Va}^{j,\varphi}(y''_N - y''_{Va})^j \quad (4)$$

in which

$${}^0G_{Hf:N}^{\varphi} = {}^0G_{Hf}^{Hcp} + m\cdot {}^0G_N^{1/2\_mol\_N_2} + a + b\cdot T$$
$${}^0G_{Hf:Va}^{\varphi} = {}^0G_{Hf}^{Hcp} + m\cdot {}^0G_{Va} \quad (5)$$

3.3 Intermetallic compounds

The intermetallic compounds Hf_3N_2 and Hf_4N_3 are modeled as stoichiometric compounds. The Gibbs energy of Hf_xN_y per mole formula, for example, is expressed by the following equation, adopting the stable structure for the elements as the thermodynamic standard state:

$$G_m^{Hf_xN_y} - x\cdot H_{Hf}^{SER} - y\cdot H_N^{SER} = A^{Hf_xN_y} + B^{Hf_xN_y}\cdot T + x\cdot {}^0G_{Hf}^{Hcp} + y\cdot {}^0G_N^{1/2\_mol\_N_2} \quad (6)$$

Usually, the model $(Me)_1(N,Va)_1$ is used to describe Fcc phase in Me-N systems. This model can cover the composition range from 0 to 50.0 at. % N. However, in Hf-N system, the Fcc phase exhibits an extensive homogeneity range from 41.5 to 52.0 at. % N, which is beyond the composition range of the model $(Hf)_1(N,Va)_1$. According to Straumanis et al. [42], there are vacancies in each of the Hf and N sublattices of the Fcc phase. Thus, the Fcc phase is modeled as $(Hf, Va)_1(N, Va)_1$. The Gibbs energy of Fcc phase can be expressed as:

$$\begin{aligned} G_m^{Fcc} - H^{SER} &= y'_{Hf} \cdot y''_N \cdot {}^0G^{Fcc}_{Hf:N} + y'_{Hf} \cdot y''_{Va} \cdot {}^0G^{Fcc}_{Hf:Va} \\ &+ y'_{Va} \cdot y''_N \cdot {}^0G^{Fcc}_{Va:N} + y'_{Va} \cdot y''_{Va} \cdot {}^0G^{Fcc}_{Va:Va} \\ &+ R \cdot T \cdot [y'_{Hf} \cdot \ln y'_{Hf} + y'_{Va} \cdot \ln y'_{Va} \\ &+ y''_N \cdot \ln y''_N + y''_{Va} \cdot \ln y''_{Va}] + {}^E G^{Fcc}_{Hf,Va:N,Va} \end{aligned} \quad (7)$$

where

$$\begin{aligned} {}^0G^{Fcc}_{Hf:N} &= a_1 + b_1 \cdot T + c_1 \cdot T \cdot \ln(T) + d_1 \cdot T^2 + e_1 \cdot T^{-1} \\ {}^0G^{Fcc}_{Hf:Va} &= {}^0G^{Fcc}_{Hf} + {}^0G_{Va} \\ {}^0G^{Fcc}_{Va:N} &= {}^0G_{Va} + {}^0G_N^{1/2\_mol\_N_2} + a_2 + b_2 \cdot T \\ {}^0G^{Fcc}_{Va:Va} &= 2 \cdot {}^0G_{Va} + a_3 + b_3 \cdot T \end{aligned} \quad (8)$$

and the excess term is given as follows:

$$\begin{aligned} {}^E G^{Fcc}_{Hf,Va:N,Va} &= y'_{Hf} \cdot y'_{Va} \cdot y''_N \cdot {}^0L^{Fcc}_{Hf,Va:N} \\ &+ y'_{Hf} \cdot y'_{Va} \cdot y''_{Va} \cdot {}^0L^{Fcc}_{Hf,Va:Va} \\ &+ y'_{Va} \cdot y''_N \cdot y''_{Va} \cdot {}^0L^{Fcc}_{Va:N,Va} \\ &+ y'_{Hf} \cdot y''_N \cdot y''_{Va} \cdot {}^0L^{Fcc}_{Hf:N,Va} \end{aligned} \quad (9)$$

In the above equations, y'_i and y''_i are the site fractions of the species in the first and second sublattices, respectively. ${}^0L^{Fcc}_{Hf,Va:N}$, ${}^0L^{Fcc}_{Hf,Va:Va}$, ${}^0L^{Fcc}_{Va:N,Va}$ and ${}^0L^{Fcc}_{Hf:N,Va}$ are the interaction parameters.

3.4 Gas phase

The gas phase is described as an ideal gas mixture of the species Hf, N, N_2 and N_3. Its Gibbs energy per mole of species is given by the following expression:

$$\begin{aligned} G^{Gas} - H^{Gas} &= \sum y_i [G_i^{Gas} - H_i^{SER} \\ &+ R \cdot T \cdot \ln(y_i)] \\ &+ R \cdot T \cdot \ln(0.98692 \cdot P / bar) \end{aligned} \quad (10)$$

$$(n^0_{Hf} + n^0_N) / n = y_{Hf} + y_N + 2 \cdot y_{N_2} + 3 \cdot y_{N_3} \quad (11)$$

where n is the number of moles of the species in the gas in internal equilibrium, $(n^0_{Hf} + n^0_N)$ is the number of moles of atoms in the gas, $y_i = (n_i / n)$ is the mole fraction of the species i, $G_i^{Gas} - H_i^{Gas}$ is the Gibbs energy of the species i, and P is the pressure. The Gibbs energy functions of the individual gas species are taken from the SGTE substances database [43].

4. Results and discussion

The assessment was carried out by using the PARRAOT module of Thermo-Calc [44] which works by minimizing the square sum of the errors. The step-by-step optimization procedure [28] was utilized in the present assessment. In the optimization, each piece of experimental information was given a certain weight based on uncertainties of the data.

The optimization starts with the thermodynamic properties of the Fcc phase. The relative enthalpies and heat capacities were calculated with parameters c_1, d_1 and e_1 in equation (8). And the parameter a_1 can be evaluated based on the data of enthalpy of formation. The end member ${}^0G^{Fcc}_{Va:Va}$ was arbitrarily given as 50*T, considering the value widely accepted for phases with A2 structure. A positive value was given to a_2 and b_2 since nitrogen with A1 structure is unstable at high temperatures. Then, the interaction parameters can be determined when optimizing the data of nitrogen pressure over Fcc phase. Good start value for the interaction parameter of liquid phase can be obtained with the pressure dependence of melting points of Fcc phase. For Hcp phase, parameters can be given based on the information of nitrogen solubility in Hcp phase and the invariant reaction liquid + Fcc = Hcp. was optimized together with phase diagram data. Next, parameters for the stoichiometric compounds were evaluated. With these reasonable start values, all the parameters were optimized simultaneously based on the experimental data to get a set of self-consistent thermodynamic parameters. The obtained parameters of the Hf-N system are listed in Table 3.

Figure 1 shows the calculated Hf-N phase diagram at pressure 1 bar N_2 along with the experimental data

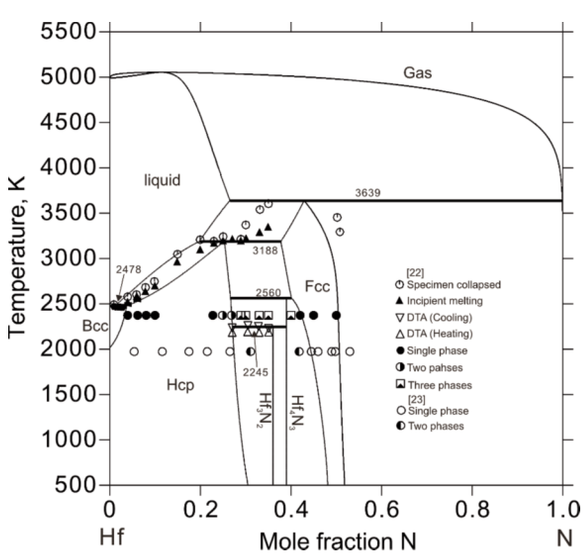

Figure 1. *Calculated phase diagram of the Hf-N system at pressure of 1 bar N_2 compared with experimental data [22, 23]*

Table 3. *Summary of the optimized thermodynamic parameters in the Hf-N system.*[a]

Fcc: Model $(Hf,Va)_1(N,Va)_1$
${}^0G^{Fcc}_{Hf:N} = -396864 + 299.124\cdot T - 49.636\cdot T\cdot \ln(T) - 0.002124\cdot T^2 + 471912\cdot T$
${}^0G^{Fcc}_{Va:N} = {}^0G_{Va} + {}^0G_N^{1/2\_mol\_N_2} + 832016 + 91.070\cdot T$
${}^0G^{Fcc}_{Va:Va} = 100\cdot T$
${}^0L^{Fcc}_{Hf:N,Va} = -43972$
${}^0L^{Fcc}_{Hf,Va:N} = -1005710$
Hcp: Model $(Hf)_1(N,Va)_{0.5}$
${}^0G^{Hcp}_{Hf:N} = {}^0G^{Hcp}_{Hf} + 0.5\cdot {}^0G_N^{1/2\_mol\_N_2} - 204434 + 46.533\cdot T$
${}^0L^{Hcp}_{Hf:N,Va} = -32931$
Bcc: Model $(Hf)_1(N,Va)_3$
${}^0G^{Bcc}_{Hf:N} = {}^0G^{Hcp}_{Hf} + 3\cdot {}^0G_N^{1/2\_mol\_N_2} + 900000 + 60\cdot T$
Hf_4N_3: Model $(Hf)_4(N)_3$
$G_m^{Hf_4N_3} - 4\cdot H_{Hf}^{SER} - 3\cdot H_N^{SER} = -153938 + 34.445\cdot T + 4\,{}^0G^{Hcp}_{Hf} + 3\cdot {}^0G_N^{1/2\_mol\_N_2}$
Hf_3N_2: Model $(Hf)_3(N)_2$
$G_m^{Hf_3N_2} - 3\cdot H_{Hf}^{SER} - 2\cdot H_N^{SER} = -144517 + 31.818\cdot T + 3\cdot {}^0G^{Hcp}_{Hf} + 2\cdot {}^0G_N^{1/2\_mol\_N_2}$
liquid: Model $(Hf,N)_1$
${}^0L^{Liquid}_{Hf,N} = -379059$

[a] All parameters are given in J/mole and temperature (T) in K. The Gibbs energies for the pure elements are from the SGTE compilation [40]. The Gibbs energies for the Gas phase are taken from SGTE substance database [43]. The parameters not presented here are evaluated to be zero.

[22, 23] and figure 2 with the gas phase suspended. As can be seen, the composition range of Fcc phase at the N-rich side is about 52 at. % N, which agrees well with the experimental results [20, 23]. At the Hf-rich side, the calculated phase boundary cannot fit the measured data very well due to the interactive influence of the Hf_4N_3 phase. This phenomenon also occurred in the Ti-N system [27]. The calculated melting point of Fcc phase at 1 bar N_2 pressure is 3639 K, which is 21 K lower than the experimental value reported by Booker and Brukl [22]. The experiments were conducted under 2 bar pressure of Ar [22], which may give an explanation for this discrepancy. For the solidus of the Hcp phase, the slope of the calculated solidus is lower than that of the experimental one [22]. However, any further attempt to improve the fit to the experimental data will cause a miscibility gap of the Hcp phase at low temperatures which has no experimental evidence. Figure 3 shows the calculated Hf-rich region of the phase diagram, the calculated temperature of invariant reaction liquid ↔ Bcc + Hcp is 15 K higher than the value reported by Booker and Brukl [22]. This can be explained by the fact that the hafnium used in their experiments contain 3.1 wt. % of zirconium. Their result of melting point of hafnium

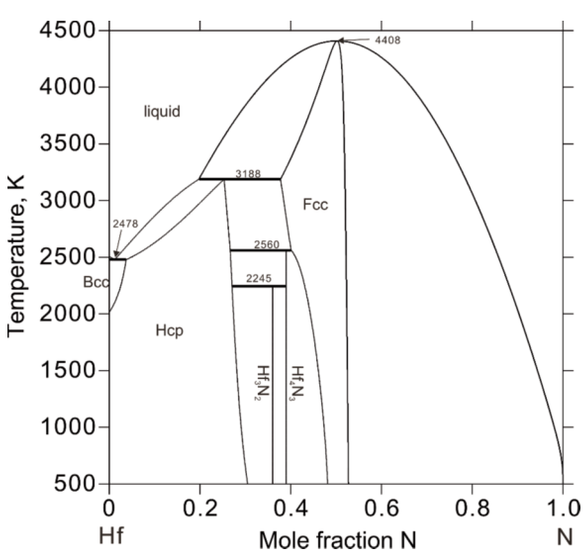

Figure 2. *Calculated phase diagram of the Hf-N system with gas phase suspended*

is also 15 K lower than the value accepted by the SGTE data for pure elements [40]. The solubility of nitrogen in Bcc phase is neglected because there is no experimental data and the solubility seems very small.

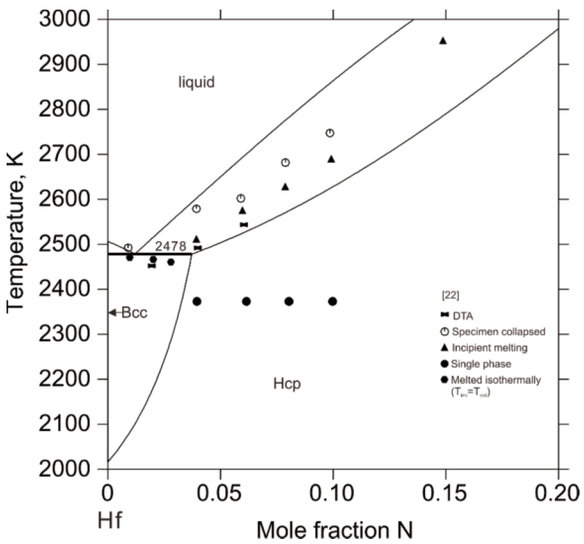

Figure 3. *Calculated Hf-rich region of the Hf-N system compared with experimental data [22].*

The calculated enthalpy of formation for Fcc (HfN) at 298 K compared with experimental [38] and first-principles calculated [10, 39] results is shown in figure 4. Although the values calculated by Gu et al. [10] are slightly smaller than other values, the tendency is the same as the present work. It can be concluded that all values agree with each other very well. Figure 5 shows the calculated heat capacity of $HfN_{1.0}$ compared with the experimental results [32, 33] and first-principles calculations [9, 15, 34]. The calculated results fit these data quite well except at very low temperatures, which is limited by the present thermodynamic model for heat capacity. Figures 6 and 7 are the calculated relative enthalpies of $HfN_{0.95}$ and $HfN_{1.09}$ compared with the experimental data [35]. Figure 8 is the calculated phase stability diagram showing the three phase equilibrium gas + liquid + Fcc compared with the experimental data [26]. As can be seen, the calculated results can well reproduce the experimental data [26]. Figure 9 shows the calculated partial equilibrium pressure of N_2 at different temperatures. The calculated results agree very well with the experimental data [36, 37] at high

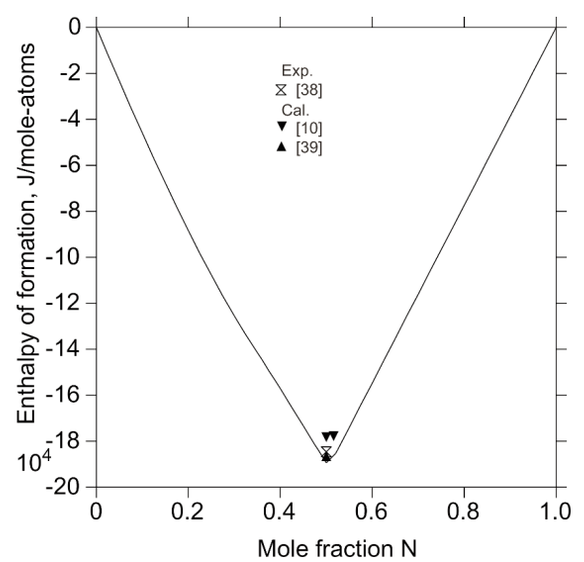

Figure 4. *Calculated enthalpy of formation at 298K along with experimental data [10, 38, 39].*

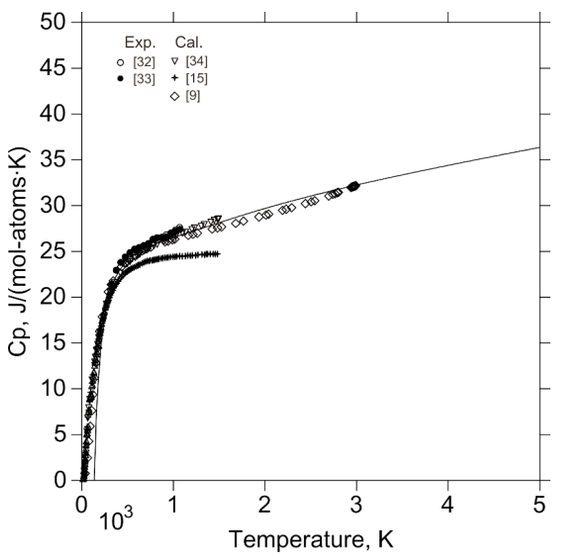

Figure 5. *Calculated heat capacity of $Hf_{0.5}N_{0.5}$ compared with experimental and first-principles calculated data [9, 15, 32-34].*

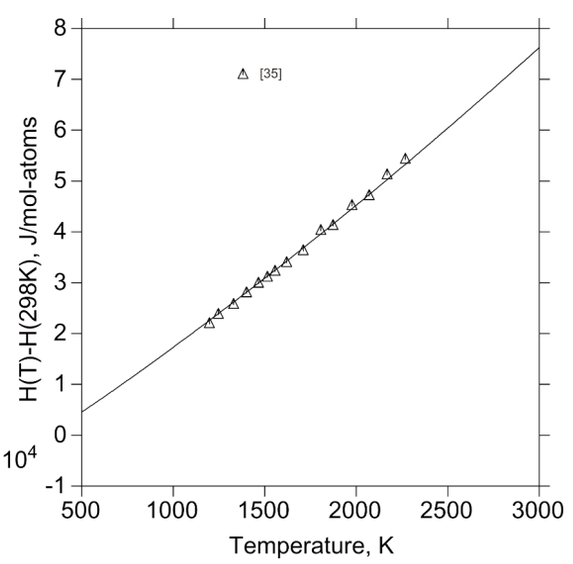

Figure 6. *The calculated heat content of HfN, H(T)-H(298), at x(N)=0.49 compared with experimental data [35].*

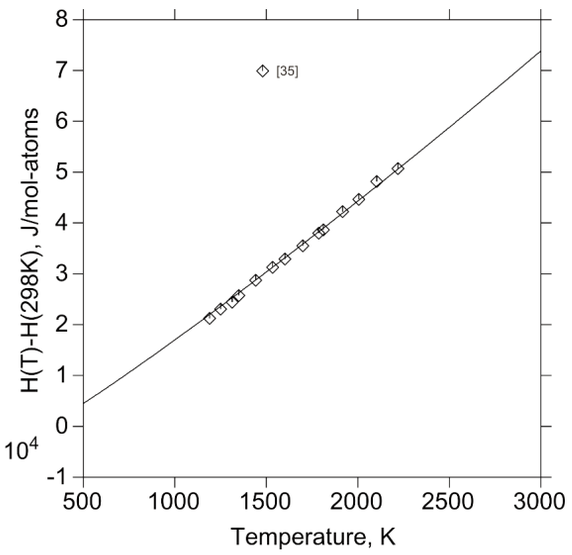

Figure 7. *Calculated heat content of HfN, H(T)-H(298), at x(N)=0.52 compared with experimental data [35].*

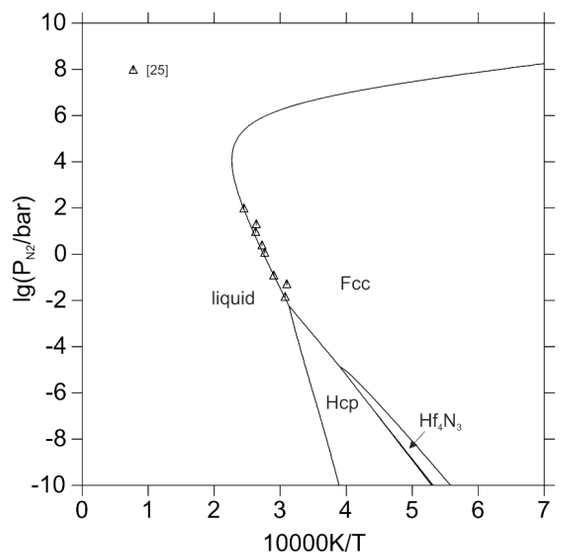

Figure 8. *Calculated phase stability diagram showing the three phases equilibrium gas + liquid + Fcc compared with experimental data [25].*

temperatures, while a small deviation between experiment and calculation occurs at lower temperatures. Such a deviation may be attributed to the fact that the diffusion of nitrogen in Fcc phase is very slow at low temperatures and thus hard to reach equilibrium.

Conclusion

All the experimental phase diagrams and thermodynamic data available in the literature for the Hf-N system have been critically evaluated. A set of self-consistent thermodynamic parameters for the Hf-N system is obtained by means of the CALPHAD method. Comprehensive comparisons show that the calculated phase diagrams and thermodynamic properties can well reproduce the experimental data.

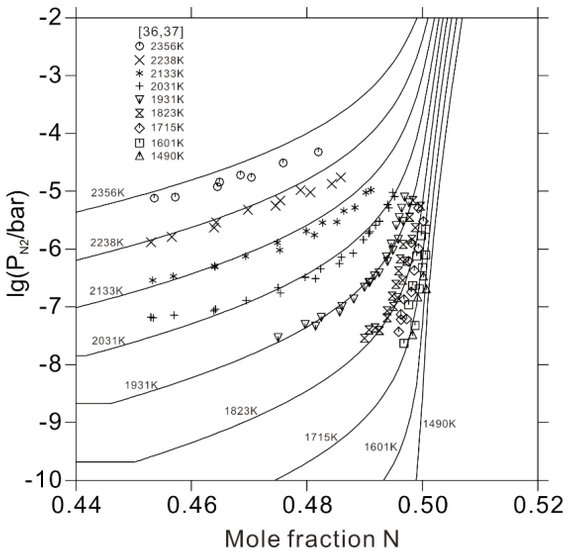

Figure 9. *Calculated partial equilibrium pressure of N_2 of Fcc phase at different temperatures compared with the experimental data [36, 37].*

Acknowledgement

The financial support from the National Natural Science Foundation of China (grant no. 51601061) is greatly acknowledged.

References

[1] S. Dong, X. Chen, X. Zhang, G. Cui, Coord. Chem. Rev., 257 (2013) 1946-1956.

[2] J. Musil, Surf. Coat. Technol., 125 (2000) 322-330.

[3] A.E. Kaloyeros, E. Eisenbraun, Annu. Rev. Mater. Sci., 30 (2000) 363-385.

[4] S.-H. Jhi, J. Ihm, S.G. Louie, M.L. Cohent, Nature (London), 399 (1999) 132-134.

[5] L. Tsetseris, N. Kalfagiannis, S. Logothetidis, S.T. Pantelides, Phys. Rev. B: Condens. Matter Mater. Phys., 76 (2007) 224107/224101-224107/224107.

[6] A.J. Perry, J. Vac. Sci. Technol., A, 6 (1988) 2140-2148.

[7] L. Tsetseris, N. Kalfagiannis, S. Logothetidis, S.T. Pantelides, Phys Rev Lett, 99 (2007) 125503.

[8] P. Kroll, Phys. Rev. Lett., 90 (2003) 125501/125501-125501/125504.

[9] X.-G. Lu, M. Selleby, B. Sundman, Acta Mater., 55 (2007) 1215-1226.

[10] Z. Gu, C. Hu, H. Huang, S. Zhang, X. Fan, X. Wang, W. Zheng, Acta Mater., 90 (2015) 59-68.

[11] W. Wei, H. Wang, Y.H. Hu, J. Mater. Chem. A, 1 (2013) 14350-14357.

[12] R.A. Araujo, X. Zhang, H. Wang, J. Vac. Sci. Technol., B: Microelectron. Nanometer Struct.—Process., Meas., Phenom., 26 (2008) 1871-1874.

[13] M.H. Staia, D.G. Bhat, E.S. Puchi-Cabrera, J. Bost, Wear, 261 (2006) 540-548.

[14] C. Escobar, M. Villarreal, J.C. Caicedo, W. Aperador, P. Prieto, Surf. Coat. Technol., 221 (2013) 182-190.

[15] B. Saha, J. Acharya, T.D. Sands, U.V. Waghmare, J. Appl. Phys., 107 (2010) 033715/033711-033715/033718.

[16] L.-Q. Chen, J. Zhu, Y.-J. Hao, L. Zhang, G. Xiang, B.-R. Yu, X.-J. Long, J. Phys. Chem. Solids, 75 (2014) 1295-1300.

[17] E. Wuchina, M. Opeka, F. Gutierrez-Mora, R.E. Koritala, K.C. Goretta, J.L. Routbort, J. Eur. Ceram. Soc., 22 (2002) 2571-2576.

[18] Y. Peng, Y. Du, P. Zhou, W. Zhang, W. Chen, L. Chen, S. Wang, G. Wen, W. Xie, International Journal of Refractory Metals & Hard Materials, 42 (2014) 57-70.

[19] H. Okamoto, Bulletin of Alloy Phase Diagrams, 11 (1990) 146-149.

[20] W. Lengauer, D. Rafaja, G. Zehetner, P. Ettmayer, Acta Mater., 44 (1996) 3331-3338.

[21] N.H. Krikorian, T.C. Wallace, J. Electrochem. Soc., 111 (1964) 1431-1433.

[22] P.H. Booker, C.E. Brukl, Rep. USAF Contract AF-33, (615)-67-C-1513, Part VI, (October 1969).

[23] E. Rudy, F. Benesovsky, Monatshefte für Chemie und verwandte Teile anderer Wissenschaften, 92 (1961) 415-441.

[24] H. Nowotny, H. Braun, F. Benesovsky, Radex Rundsch., (1960) 367-372.

[25] M.A. Eron'yan, R.G. Avarbe, I.N. Danisina, Teplofiz. Vys. Temp., 14 (1976) 398-399.

[26] P. Ettmayer, R. Kieffer, F. Hattinger, Metall (Berlin), 28 (1974) 1151-1156.

[27] S. Jonsson, Z. Metallkd., 87 (1996) 691-702.

[28] Y. Du, R. Schmid-Fetzer, H. Ohtani, Z. Metallkd., 88 (1997) 545-556.

[29] E.K. Storms, U. S. A. E. C., LA-2942 (1964) 245.

[30] E. Rudy, Met. Trans., 1 (1970) 1249-1252.

[31] M. Billy, B. Teyssedre, Bull. Soc. Chim. Fr., (1973) 1537-1540.

[32] H.L. Schick, Editor, Thermodynamics of Certain Refractory Compounds. Vol. 2: Thermodynamic Tables, Bibliography, and Property File, Academic Press, London, 1966.

[33] W. Lengauer, S. Binder, K. Aigner, P. Ettmayer, A. Guillou, J. Debuigne, G. Groboth, J. Alloys Compd., 217 (1995) 137-147.

[34] A. Wang, S. Shang, D. Zhao, J. Wang, L. Chen, Y. Du, Z.-K. Liu, T. Xu, S. Wang, Calphad, 37 (2012) 126-131.

[35] V.F. Litvinenko, A.S. Bolgar, O.P. Kulik, O.T. Khorpyakov, Zh. Fiz. Khim., 53 (1979) 318-321.

[36] G.M. Kibler, T.F. Lyon, M.J. Linevsky, V.J. DeSantis, Rep. Contract AF-33, (616)-6841, Part III, (March 1964).

[37] G.M. Kibler, T.F. Lyon, M.J. Linevsky, V.J. DeSantis, Rep. Contract AF-33, (616)-6841, Part IV, (August 1964).

[38] G.L. Humphrey, J. Am. Chem. Soc., 75 (1953) 2806-2807.

[39] A.M. Mulokozi, J. Less-Common Met., 79 (1981) 139-143.

[40] A.T. Dinsdale, CALPHAD: Comput. Coupling Phase Diagrams Thermochem., 15 (1991) 317-425.

[41] O. Redlich, A.T. Kister, Ind. Eng. Chem., 40 (1948) 84,85-88.

[42] M.E. Straumanis, C.A. Faunce, Z. Anorg. Allg. Chem., 353 (1967) 329-336.

[43] S.S. Database, Thermo-calc Company, (2008).

[44] B. Sundman, B. Jansson, J.O. Andersson, CALPHAD: Comput. Coupling Phase Diagrams Thermochem., 9 (1985) 153-190.

[45] H. King, Bulletin of alloy phase diagrams, 2 (1981) 401-402.

[46] R.G. Ross, W. Hume-Rothery, J. Less-Common Met., 5 (1963) 258-270.

[47] A.N. Christensen, Acta Chem. Scand., 44 (1990) 851-852.

TERMODINAMIČKO MODELOVANJE HF-N SISTEMA

M. Pang [a], Y. Peng [b,*], P. Zhou [c], Y. Du [a]

[a] Centralni južni Univerzitet, Državna ključna laboratorija za metalurgiju praha, Changsha, Kina
[b] Hunan Univerzitet tehnologije, Fakultet za metalurgiju i inženjerstvo materijala, Zhuzhou, Kina
[c] Hunan Univerzitet za nauku i tehnologiju, Mašinski i elektrotehnički fakultet, Xiangtan, Kina

Apstrakt

Hf-N legure se koriste i pručavaju u oblasti elektronskih uređaja i proizvodnji alata za rezanje. Termodinamički opis ovog sistema je ključan za dalji razvoj ovih legura. Termodinamičko modelovanje Hf-N sistema je izvršeno CALPHAD metodom i bazirano je na dostupnim podacima faznog dijagrama, kao i na podacima o termodinamičkim osobinama. Fcc faza je modelirana kao (Hf, Va)1(N, Va)1 da obuhvati celokupan sastav, zbog toga što je dobijeno da je rastvorljivost azota u Fcc fazi oko 52 at.%. Dobijen je skup termodinamičkih parametara za Hf-N sistem. Izračunati fazni dijagrami i termodanimačke veličine na osnovu prisutnih parametara, slažu se sa podacima dobijenim tokom eksperimenta.

Ključne reči: *CALPHAD; Hf-N; Fazni dijagram; Hafnijum nitridi.*